

**INPUT IMPEDANCE ANALYSIS OF A  
MICROSTRIP ANNULAR-RING ANTENNA  
WITH A THICK SUBSTRATE**

*H. Liu and X.-F. Hu*

- 1. Introduction**
  - 2. Formulation**
  - 3. Galerkin's Method and Characteristic Equation for Eigenvalue**
  - 4. Fields Excited by the Probe**
  - 5. Galerkin's Method with Singularity Subtraction**
  - 6. Input Impedance of the Probe Excited Antenna**
  - 7. Results and Discussions**
  - 8. Conclusion**
- Appendix A**  
**Acknowledgment**  
**References**

**1. Introduction**

While the rectangular and circular patches are probably the most extensively studied patch shapes [1–6], the annular ring patch has also received considerable attention [7–13]. There are several interesting features associated with this patch, First, for a given frequency, the size is substantially smaller than that of the circular patch when both operated in the lowest mode. Second, it can be easily designed for dual band operation by using a concentric ring structure [9], or by employing another circular patch [11]. The lowest mode has a very narrow operating band, but the bandwidth is substantially increased when operated in some high modes [10,17]. In [7,9], the authors analyzed the annular ring structure by using an equivalent circuit modal based on a

transmission line analysis. A spectral domain approach was carried out in [8] but no attempt was made to model the feed structure. In [10], the authors treated the structure as a magnetic wall cavity and, the vector integral equations were established and the resonant wavenumber has been strictly evaluated, but the input impedance has been calculated rather crudely by employing the single mode approximation (SMA) method.

In this paper we shall present a method to calculate the surface current and the input impedance of an annular ring microstrip antenna excited by a probe. This method, which has been used effectively to calculate the input impedance of a circular patch antenna [6], is beyond the range of validity of the SMA method in [10]. Higher modes effect of the surface current on the patch and the surface wave due to the dielectric substrate have been included in the analysis. To do this, we first formulate the mixed boundary value problem for an annular ring conductor printed on a dielectric substrate backed by a ground plane. Expanding the unknown surface current, both TE and TM modes, into a series containing the eigen functions of the magnetic-wall cavity [2], the mixed boundary value problem is reduced to the solution of a set of dual integral equation. The resonant wave number is obtained from the characteristic equation. Second, we calculate the incident field on the patch generated by the probe current, together with the field generated by the induced current on the patch. By imposing the boundary condition on the patch, the scattering equation of the problem is established. Finally, by applying Galerkin's method, the unknown surface current on the annular ring patch can then be solved. The input impedance can be derived from the surface current.

## 2. Formulation

Assume an annular ring carries an arbitrary distribution of current be placed at a distance  $d$  from the surface of dielectric substrate backed by a ground plane, as shown in Fig. 1. Using the vector Hankel transform (VHT) [4], the transverse electric field and electric current can be expressed as

$$\mathbf{e}_n(\rho) = \int_0^\infty dk_\rho k_\rho \bar{\mathbf{H}}_n(k_\rho \rho) \cdot \bar{\mathbf{G}}(k_\rho) \cdot \mathbf{K}_n(k_\rho) \quad (1)$$

$$\mathbf{k}_n(\rho) = \int_0^\infty dk_\rho k_\rho \overline{\mathbf{H}}_n(k_\rho \rho) \cdot \mathbf{K}_n(k_\rho) \quad (2)$$

where

$$\mathbf{e}_n(\rho) = \begin{bmatrix} E_{\rho n}(\rho)/\cos n\phi \\ -E_{\phi n}(\rho)/\sin n\phi \end{bmatrix}, \quad \mathbf{k}_n(\rho) = \begin{bmatrix} -K_{\rho n}(\rho)/\cos n\phi \\ K_{\phi n}(\rho)/\sin n\phi \end{bmatrix} \quad (3)$$

is relate to the  $n$ th harmonic of the electric field and electric current on the patch, respectively.

$$\mathbf{K}_n(k_\rho) = \begin{bmatrix} K_{n1}(k_\rho) \\ K_{n2}(k_\rho) \end{bmatrix} \quad (4)$$

is the VHT of the electric current  $k_n(\rho)$  on the patch,

$$\overline{\mathbf{H}}_n(k_\rho \rho) = \begin{bmatrix} J'n(k_\rho \rho) & \frac{n}{k_\rho \rho} J_n(k_\rho \rho) \\ \frac{n}{k_\rho \rho} J_n(k_\rho \rho) & J'n(k_\rho \rho) \end{bmatrix} \quad (5)$$

is the kernel of the vector Hankel transform, and

$$\overline{\mathbf{G}}_n(k_\rho) = \begin{bmatrix} \frac{k_z}{2\omega\varepsilon}(1 - R^{TM}) & 0 \\ 0 & \frac{\omega\mu}{2k_z}(1 + R^{TE}) \end{bmatrix} \quad (6)$$

is the dyadic Green's function for the  $\rho$  and  $\phi$  components of the current in the VHT spectral space. In the above,  $R^{TM}$  and  $R^{TE}$  are generalized reflection coefficients for TM and TE waves, respectively. They can be expressed as

$$R^{TM} = \frac{i\varepsilon_1 k_z \cos k_{1z}d - \varepsilon k_{1z} \sin k_{1z}d}{i\varepsilon_1 k_z \cos k_{1z}d + \varepsilon k_{1z} \sin k_{1z}d} \quad (7)$$

$$R^{TE} = \frac{i\mu_1 k_z \cos k_{1z}d + \mu k_{1z} \sin k_{1z}d}{i\mu_1 k_z \cos k_{1z}d - \mu k_{1z} \sin k_{1z}d} \quad (8)$$

where

$$k_i = \omega^2 \mu_i \varepsilon_i, \quad k_{iz} = \sqrt{k_i^2 - k_\rho^2}, \quad i = 0, 1 \quad (9)$$

and  $d$  is the substrate thickness. Imposing the mixed boundary conditions on the plane  $z = 0$ , we have

$$\mathbf{e}_n(\rho) = 0, \quad a_1 < \rho < a_2 \tag{10}$$

$$\mathbf{k}_n(\rho) = 0, \quad \text{elsewhere} \tag{11}$$

where  $\mathbf{e}_n(\rho)$  and  $\mathbf{k}_n(\rho)$  are given by (1) and (2), respectively.

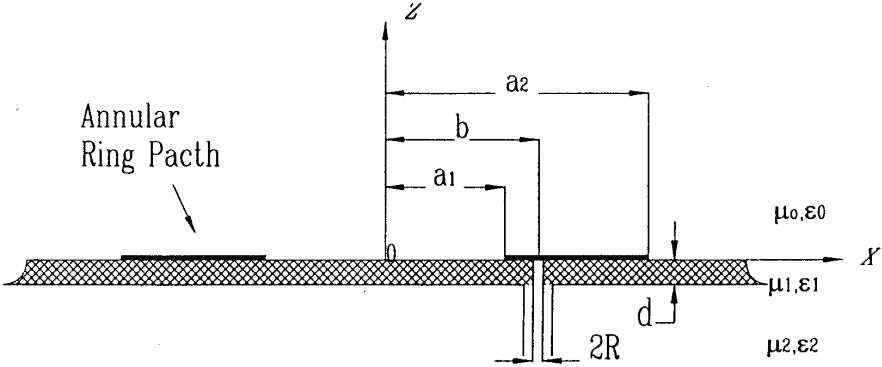


Figure 1. Microstrip annular ring antenna excited by a probe.

### 3. Galerkin's Method and Characteristic Equation for Eigenvalue

In (1) and (2), the current distribution  $\mathbf{k}_n(\rho)$  or its VHT  $\mathbf{K}_n(k\rho)$  is unknown. We can expand the unknowns into a series of basis function based on the magnetic-wall cavity modal [2,10]. Then the unknowns can be solved by using Galerkin's method.

The current on the annular patch corresponding to the field of  $\text{TM}_{nm}$  modes in a magnetic-wall-cavity is

$$\mathbf{k}_n(\rho) = \begin{cases} a_m \bar{\psi}_{nm}(\rho), & a_1 < \rho < a_2 \\ 0, & \text{elsewhere} \end{cases} \tag{12}$$

where

$$\bar{\psi}_{nm}(\rho) = \begin{bmatrix} \psi'_n(\beta_{nm}\rho/a_1) \\ \frac{na_1}{\beta_{nm}\rho} \psi_n(\beta_{nm}\rho/a_1) \end{bmatrix} \tag{13}$$

$$\psi_n(\beta_{nm}\rho/a_1) = J_n(\beta_{nm}\rho/a_1)N'_n(\beta_{nm}) - J'_n(\beta_{nm})N_n(\beta_{nm}\rho/a_1) \quad (14)$$

where  $\beta_{nm}$  is the  $m$ th root of  $\psi'_n(\beta_{nm}c) = 0$  where  $c = a_2/a_1$ . The VHT of  $\mathbf{k}_n(\rho)$  in (12) can be derived as

$$\mathbf{K}_n(k_\rho) = a_m \Psi_{nm}(k_\rho) \quad (15)$$

where

$$\Psi_{nm}(k_\rho) = \begin{bmatrix} \frac{\beta_{nm}/a_1}{(\beta_{nm}/a_1)^2 - k_\rho^2} Y'_{nm}(k_\rho) \\ \frac{na_1}{k_\rho \beta_{nm}} Y_{nm}(k_\rho) \end{bmatrix} \quad (16)$$

$$Y_{nm}(k_\rho) = \psi_n(\beta_{nm}c)J_n(k_\rho a_2) - \psi_n(\beta_{nm})J_n(k_\rho a_1) \quad (17)$$

For completeness, we have to include the current corresponding to the TE mode of the magnetic-wall-cavity. The current on the annular ring corresponding to the field of TE <sub>$np$</sub>  modes can be written as

$$\mathbf{k}_n(\rho) = \begin{cases} b_p \bar{\phi}_{np}(\rho), & a_1 < \rho < a_2 \\ 0, & \text{elsewhere} \end{cases} \quad (18)$$

where

$$\bar{\phi}_{np}(\rho) = \begin{bmatrix} \frac{na_1}{\alpha_{np}\rho} \phi_n(\alpha_{np}\rho/a_1) \\ \phi'_n(\alpha_{np}\rho/a_1) \end{bmatrix} \quad (19)$$

and

$$\phi_n(\alpha_{np}\rho/a_1) = J_n(\alpha_{np}\rho/a_1)N_n(\alpha_{np}) - J_n(\alpha_{np})N_n(\alpha_{np}\rho/a_1) \quad (20)$$

where  $\alpha_{np}$  is the  $p$ th root of the equation  $\phi_n(\alpha_{np}c) = 0$ . The VHT of  $\mathbf{k}_n(\rho)$  in (18) can be derived to be

$$\mathbf{K}_n(k_\rho) = b_p \Phi_{np}(k_\rho) \quad (21)$$

where

$$\Phi_{np}(k_\rho) = \left[ \frac{k_\rho a_1}{k_\rho^2 - (\alpha_{np}/a_1)^2} Z_{np}(k_\rho) \right] \quad (22)$$

and

$$Z_{np}(k_\rho) = c\phi'_n(\alpha_{np}c)J_n(k_\rho a_2) - \phi'_n(\alpha_{np})J_n(k_\rho a_1) \quad (23)$$

An orthogonal set of vector basis function approaching the current distribution on the antenna patch can be written as

$$\mathbf{k}_n(\rho) = \begin{cases} \sum_{m=1}^M a_m \bar{\psi}_{nm}(\rho) + \sum_{p=1}^P b_p \bar{\phi}_{np}(\rho), & a_1 < \rho < a_2 \\ 0, & \text{elsewhere} \end{cases} \quad (24)$$

and its VHT form is

$$\mathbf{K}_n(k_\rho) = \sum_{m=1}^M a_m \Psi_{nm}(k_\rho) + \sum_{p=1}^P b_p \Phi_{np}(k_\rho) \quad (25)$$

We note that with the form of (24), the boundary condition in (11) is always ensured. Now, by making use of (10), and recalling (1), we have the characteristic equation expressed as

$$\int_0^\infty dk_\rho k_\rho \bar{\mathbf{H}}_n(k_\rho \rho) \cdot \bar{\mathbf{G}}(k_\rho) \cdot \mathbf{K}_n(k_\rho) = 0 \quad (26)$$

Substitute (25) into (26) and multiply both sides of (26) by  $\rho\psi_{nj}^t$  and  $\rho\phi_{nk}^t$ , respectively. The superscript  $t$  implies transpose. Integrating with respect to  $\rho$  from  $a_1$  and  $a_2$ , we have, after invoking Parseval's theorem

$$\left. \begin{aligned} \sum_{m=1}^M a_m A_{jm}^{\psi\psi} + \sum_{p=1}^P b_p A_{jp}^{\psi\phi} &= 0, \quad j = 1, 2, \dots, M \\ \sum_{m=1}^M a_m A_{km}^{\phi\psi} + \sum_{p=1}^P b_p A_{kp}^{\phi\phi} &= 0, \quad k = 1, 2, \dots, P \end{aligned} \right\} \quad (27)$$

where

$$A_{ij}^{\psi\psi} = \int_0^\infty dk_\rho k_\rho \Psi_{ni}^t(k_\rho) \cdot \overline{\mathbf{G}}(k_\rho) \cdot \Psi_{nj}(k_\rho) \quad (28)$$

$$A_{ij}^{\psi\phi} = A_{ji}^{\phi\psi} = \int_0^\infty dk_\rho k_\rho \Psi_{ni}^t(k_\rho) \cdot \overline{\mathbf{G}}(k_\rho) \cdot \Phi_{nj}(k_\rho) \quad (29)$$

$$A_{ij}^{\phi\phi} = \int_0^\infty dk_\rho k_\rho \Phi_{ni}^t(k_\rho) \cdot \overline{\mathbf{G}}(k_\rho) \cdot \Phi_{nj}(k_\rho) \quad (30)$$

Nontrivial solution can exist if the determinant of Eq. (27) vanishes, that is

$$\det \left[ A_{ij} \right] = f(k_{1R}) = 0 \quad (31)$$

Thus the resonant wave number  $k_{1R}$  is evaluated. Generally,  $k_{1R}$  is complex with a small negative imaginary part. This negative imaginary part accounts for the radiation loss.

#### 4. Fields Excited by the Probe

We wish to obtain the field solution of a printed antenna under a probe excitation. To do this we have to obtain the primary field in the upper half-space due to a finite-radius vertical probe embedded in the first layer of a stratified half-space as shown in Fig. 2. Using the dyadic Green's function formalism we can show that the  $\mathbf{z}$ -component of the electric field, due to a vertical probe of length  $L$  and radius  $R$  with uniform current  $I$  in an unbounded medium  $\varepsilon_1, \mu_1$ , is [5]

$$E_{1z}^P = \frac{-IL}{4\pi\omega\varepsilon_1} \int_0^\infty dk_\rho \frac{k_\rho^3}{k_{1z}} \text{sinc} \left( \frac{k_{1z}L}{2} \right) e^{\pm ik_{1z}(z+\frac{d}{2})} J_0(k_\rho\rho) J_0(k_\rho R), \quad \left| z + \frac{d}{2} \right| > \frac{L}{2} \quad (32)$$

where  $\text{sinc}(x) = \sin(x)/x$ , and the superscript  $P$  stands for the probe. The upper sign is chosen when  $z > -(d-L)/2$  and the lower for  $z < -(d+L)/2$ . Using the transmission and reflection properties of cylindrical waves [14] we conclude that the field in the upper half-space is

$$E_{1z}^P = \frac{-IL}{4\pi\omega\epsilon_1} \int_0^\infty dk_\rho \frac{k_\rho^3}{k_{1z}} \text{sinc}\left(\frac{k_{1z}L}{2}\right) e^{ik_{1z}(z+\frac{d}{2})} \cdot J_0(k_\rho\rho)J_0(k_\rho R) \frac{(1 + R_{12}^{TM}e^{ik_{1z}d})X_{10}^{TM}}{1 - R_{10}^{TM}R_{12}^{TM}e^{2ik_{1z}d}} \quad (33)$$

where

$$R_{ij}^{TM} = \frac{\epsilon_j k_{iz} - \epsilon_i k_{jz}}{\epsilon_j k_{iz} + \epsilon_i k_{jz}}, \quad X_{ij}^{TM} = 1 + R_{ij}^{TM} \quad (34)$$

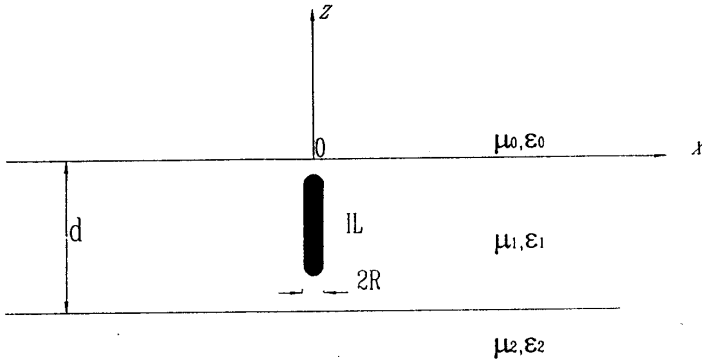


Figure 2. A probe embedded in a stratified medium.

In a printed patch antenna application  $\epsilon_2, \mu_2$ , correspond to a highly conductive ground plane implying that  $R_{12}^{TM} \cong 1$  and  $L = d$ . For a probe location at  $\bar{\rho} = \hat{x}b$ , using the addition theorem[18], we have the field transverse to  $z$  direction due to the probe ([15], p.215):

$$\mathbf{E}_s^P = \hat{\rho} \sum_{n=0}^\infty \cos n\phi \int_0^\infty dk_\rho ik_z P_n(k_\rho) J_n'(k_\rho\rho) e^{ik_z z} - \hat{\phi} \sum_{n=0}^\infty \sin n\phi \int_0^\infty dk_\rho ik_z P_n(k_\rho) \frac{nJ_n(k_\rho\rho)}{k_\rho\rho} e^{ik_z z} \quad (35)$$

Since the harmonics are orthogonal to each other, we need only to look at each of them independently. In terms of VHT the  $n$ th harmonic in (35) when  $z = 0$  can be written as

$$\mathbf{e}_n^P(\rho) = \begin{bmatrix} E_{\rho n}(\rho)/\cos n\phi \\ -E_{\phi n}(\rho)/\sin n\phi \end{bmatrix} = \int_0^\infty dk_\rho k_\rho \bar{\mathbf{H}}_n(k_\rho \rho) \cdot \mathbf{S}_n(k_\rho) \quad (36)$$

where

$$\mathbf{S}_n(k_\rho) = \frac{I}{2\pi} (2 - \delta_{0n}) J_0(k_\rho R) J_n(k_\rho b) \frac{k_\rho}{k_{1z}^2} \bar{\mathbf{G}}(k_\rho) \cdot \begin{bmatrix} 1 \\ 0 \end{bmatrix} \quad (37)$$

Now we have derived the expression of the transverse field on the printed patch, it comes from two sources: the incident field excited by the current  $I$  on the probe and the field produced by the induced current  $\mathbf{k}_n(\rho)$  on the patch. Substitute (36) into (10) and (11), and take into account of the copper loss on the patch, we have

$$\left. \begin{aligned} \mathbf{e}_n^P(\rho) + \mathbf{e}_n(\rho) &= -Z_s \mathbf{k}_n(\rho), & a_1 < \rho < a_2 \\ \mathbf{k}_n(\rho) &= 0, & \text{elsewhere} \end{aligned} \right\} \quad (38)$$

namely

$$\int_0^\infty dk_\rho k_\rho \bar{\mathbf{H}}_n(k_\rho \rho) \cdot \bar{\mathbf{G}}(k_\rho) \cdot \mathbf{K}_n(k_\rho) + \int_0^\infty dk_\rho k_\rho \bar{\mathbf{H}}_n(k_\rho \rho) \cdot \mathbf{S}_n(k_\rho) = -Z_s \mathbf{k}_n(\rho), \quad a_z < \rho < a_2 \quad (39a)$$

$$\int_0^\infty dk_\rho k_\rho \bar{\mathbf{H}}_n(k_\rho \rho) \cdot \mathbf{K}_n(k_\rho) = 0, \quad \text{elsewhere} \quad (39b)$$

where  $Z_s = \sqrt{\omega\mu/i\sigma}$  is the surface impedance of the printed patch due to the finite conductivity of the metallic patch. From (39), with the exciting current  $I$  on the probe the unknown current distribution  $\mathbf{k}_n(\rho)$  can be solved.

## 5. Galerkin's Method with Singularity Subtraction

When the microstrip patch is being excited by a probe as shown in Fig. 1, the current distribution on the patch in the vicinity of the probe has a singularity due to the singular nature of the field around the probe, which result in slow convergence in Eq. (39). This case can be improved by decomposing the patch current into two parts. The first part contains the singular nature of the feed point and, satisfies the boundary condition, while the second part needs only to satisfy the boundary condition. Thereby

$$\mathbf{J}_s(\rho) = \mathbf{J}_s^S(\rho) + \mathbf{J}_s^R(\rho) \quad (40)$$

Where  $\mathbf{J}_s^S$  and  $\mathbf{J}_s^R$  stand for the singular and regular parts of the patch current, respectively.  $\mathbf{J}_s^S$  can be chosen as the patch current of a lossy cavity with magnetic-wall under a probe excitation in order to accelerate the convergence [5], and  $\mathbf{J}_s^R$  can be chosen in the form of (24). Under such circumstances, we note that (39b) is always ensured. Therefore we need only to concentrate on Eq. (39a). For brevity, we only write the VHT of the  $n$ th harmonic of  $\mathbf{J}_s^S$  here, the derivation of  $\mathbf{J}_s^S$  can be found in **Appendix A**, that is

$$\begin{aligned} \mathbf{K}_n^S(k_\rho) &= \frac{I}{2\pi}(2 - \delta_{0n}) \frac{k_\rho J_0(k_\rho R) J_n(k_\rho b)}{k_\rho^2 - k_{1s}^2} \begin{bmatrix} 1 \\ 0 \end{bmatrix} \\ &+ \frac{I}{4}(2 - \delta_{0n}) i k_{1s} J_0(k_{1s} R) \begin{bmatrix} K_n^{(1)}(k_\rho) \\ K_n^{(2)}(k_\rho) \end{bmatrix} \end{aligned} \quad (41)$$

In order to accelerate the convergence of Eq. (39),  $k_{1s}$  in (41) can be chosen to be the wave number of the magnetic-wall-cavity filled with lossy medium, so that

$$k_{1s} = \frac{k_1}{k_{1R}} \frac{\beta_{nm}}{a_1} \quad (42)$$

where  $k_{1R}$  is the resonant wavenumber of the microstrip patch resonator predicted by Eq. (31). The expression in (41) consists of both the singular and the reflected wave terms. Considering the excitation and using the singularity subtraction, we can rewrite (39a) as

$$\begin{aligned}
& \int_0^\infty dk_\rho k_\rho \overline{\mathbf{H}}_n(k_\rho \rho) \cdot \overline{\mathbf{GZ}}(k_\rho) \cdot \mathbf{K}_n^R(k_\rho) \\
&= - \int_0^\infty dk_\rho k_\rho \overline{\mathbf{H}}_n(k_\rho \rho) \cdot (\mathbf{S}_n(k_\rho) + \overline{\mathbf{GZ}}(k_\rho) \cdot \mathbf{K}_n^S(k_\rho)) \quad (43)
\end{aligned}$$

where

$$\overline{\mathbf{GZ}}(k_\rho) = \overline{\mathbf{G}}(k_\rho) + \overline{\mathbf{I}}Z_s \quad (44)$$

where  $\mathbf{K}_n^R(k_\rho)$  and  $\mathbf{K}_n^S(k_\rho)$  stand for the VHT of the regular and the singular term of the induced currents on the patch, respectively.  $\overline{\mathbf{I}}$  is the unit dyad. Equation (43) can be converted to a matrix equation by applying Galerkin's method similar to that in deriving (27), we have

$$\left. \begin{aligned}
& \sum_{m=1}^M a_m A_{jm}^{\psi\psi} + \sum_{p=1}^P b_p A_{jp}^{\psi\phi} = B_j^\psi, \quad j = 1, 2, \dots, M \\
& \sum_{m=1}^M a_m A_{km}^{\phi\psi} + \sum_{p=1}^P b_p A_{kp}^{\phi\phi} = B_k^\phi, \quad k = 1, 2, \dots, P
\end{aligned} \right\} \quad (45)$$

where the matrix element  $A_{ij}$  can be obtained from (28) through (30) with  $\overline{\mathbf{G}}$  replaced by  $\overline{\mathbf{GZ}}$ , and

$$\begin{aligned}
B_j^\psi &= - \int_0^\infty dk_\rho k_\rho \Psi_n^t(k_\rho) \cdot (\mathbf{S}_n(k_\rho) + \overline{\mathbf{GZ}}(k_\rho) \cdot \mathbf{K}_n^S(k_\rho)) \\
B_k^\phi &= - \int_0^\infty dk_\rho k_\rho \Phi_n^t(k_\rho) \cdot \overline{\mathbf{GZ}}(k_\rho) \cdot \mathbf{K}_n^S(k_\rho)
\end{aligned}$$

Equation (45) constitutes a system of  $M+P$  linear algebraic equations and can be solved by first obtaining its elements through numerical integration. From (45), the unknowns  $(a_m, b_p)$  can be solved, and the surface current can be evaluated by substituting  $(a_m, b_p)$  into (24), in conjunction with (40).

## 6. Input Impedance of the Probe Excited Antenna

After the patch current have been evaluated, the input impedance of the microstrip annular ring antenna under a probe excitation can be derived. A stationary formula for  $Z_{in}$  is [15]

$$Z_{in} = -\frac{1}{I^2} \int_{V'} \mathbf{E}_1 \cdot \mathbf{J} dV' \quad (46)$$

Where  $V'$  is the region where  $\mathbf{J}$  distributes,  $\mathbf{J}$  is the current on the probe and  $\mathbf{E}_1$  is the total electric field in the substrate layer. The electric field inside the cavity is contributed from two sources: the current on the patch and the current on the probe, namely

$$\mathbf{E}_1 = \mathbf{E}_1^P + \mathbf{E}_1^S \quad (47)$$

where  $\mathbf{E}_1^S$  and  $\mathbf{E}_1^P$  designate the field produced by the induced surface current on the patch and the exciting current on the probe, respectively. Therefore Eq. (46) can be written as

$$Z_{in} = -\frac{1}{I^2} \int_{V'} \mathbf{E}_1^P \cdot \mathbf{J} dV' - \frac{1}{I^2} \int_{V'} \mathbf{E}_1^S \cdot \mathbf{J} dV' \quad (48)$$

The first item is relate to the self impedance of the feeding probe and, for  $e^{-i\omega t}$  dependence, it can be well approximated by [16],

$$Z_p = \frac{1}{4} \omega \mu d J_0(k_1 R) H_0^{(1)}(k_1 R) \quad (49)$$

Since the probe is assumed to have only a uniform  $z$ -component of  $\mathbf{J}$  in (48), Hence The electric field due to the induced current on the patch is given by [5]

$$E_{1z}^S = \sum_{n=0}^{\infty} \frac{i \cos n\phi}{2\omega\epsilon_1} \int_0^{\infty} dk_{\rho} k_{\rho}^2 K_{n1}(k_{\rho}) \left( e^{ik_{1z}z} + R_{12}^{TM} e^{ik_{1z}(z+d)} \right) \cdot \frac{1 + R^{TM}}{1 + R_{12}^{TM} e^{2ik_{1z}d}} J_n(k_{\rho}\rho) \quad (50)$$

where  $K_{n1}(k_{\rho})$  denotes the first element of the vector  $\mathbf{K}_n(k_{\rho})$ , with the probe current distribution given by

$$\mathbf{J} = \frac{\delta(|\bar{\rho} - \hat{x}b| - R)}{2\pi|\bar{\rho} - \hat{x}b|} B\left(\frac{2z}{d} + 1\right) I\hat{z} \quad (51)$$

where  $B(x)$  is a box function defined as zero when  $|x| > 1$ . Making use of (48)–(51), we can obtain the input impedance after some algebraic manipulation as

$$Z_{in} = Z_p + \frac{1}{2\omega\varepsilon I} \sum_{n=0}^N \int_0^\infty dk_\rho k_\rho^2 K_{n1}(k_\rho) \frac{k_z(1 - R^{TM})}{k_1^2 - k_\rho^2} J_0(k_\rho R) J_n(k_\rho b) \quad (52)$$

where

$$K_{n1}(k_\rho) = K_{n1}^S(k_\rho) + K_{n1}^R(k_\rho) = K_{n1}^S(k_\rho) + \sum_{m=1}^M a_{nm} \bar{\psi}_{nm1}(k_\rho) \quad (53)$$

where  $a_{nm}$  is obtained by solving Eq. (45).

## 7. Results and Discussions

The surfaces current expansion coefficients  $a_{nm}$  derived from (45) are used in (24) and (40) to compute the surface current on the annular ring patch, and in (52) to compute the input impedance.

Figure 3 is a vector plot showing the surface current distribution on the annular ring patch. Figure 4 shows the  $|\mathbf{J}|$  component distribution along the  $x$ -axis when the structure is at resonance,  $f = 2.88$  GHz, and at off-resonance,  $f = 2.8$  GHz. From the plots, the singularity at the feed point is clearly depicted. In Figure 4, we note that at resonance, the eigen modes of the structure are highly excited while at off-resonance these modes are poorly excited. This indicates that the  $\text{TM}_{11}$  mode of an annular-ring structure is a high quality resonator at such a thin substrate.

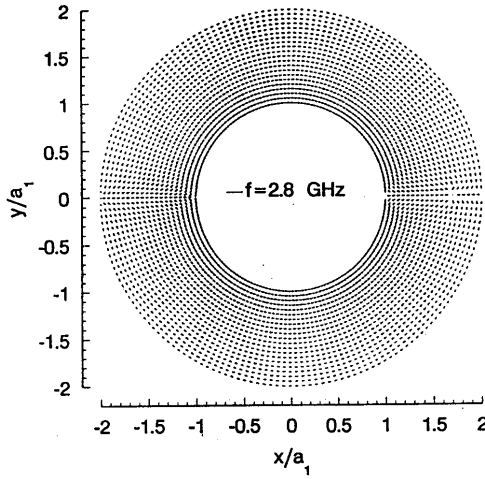


Figure 3. Surface current distribution on an annular ring patch operated at  $\text{TM}_{11}$  mode,  $f = 2.80$  GHz.  $R = 0.1$  mm,  $a_1 = 7.1$  mm,  $a_2 = 2a_1$ ,  $d = 0.05a_1$ ,  $b = 1.7a_1$ ,  $\epsilon_r = 2.65$ ,  $\sigma = 5.8 \times 10^7$ ,  $\tan \delta = 10^{-3}$ . The number of basis function are:  $M = 1$ ,  $P = 0$ , and  $N = 50$ .

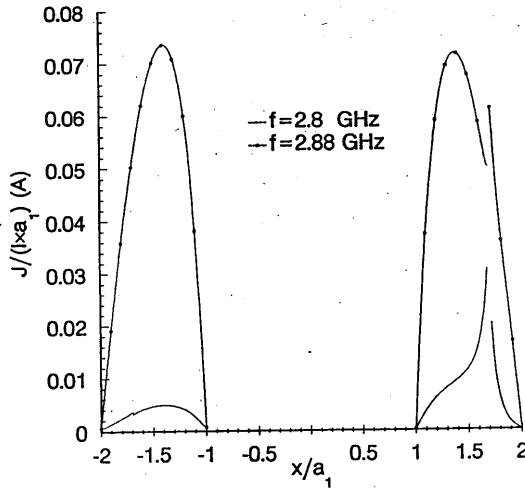


Figure 4. Current distribution along  $x$ -axis at resonance,  $f = 2.88$  GHz, and at off-resonance,  $f = 2.80$  GHz. Parametric values are the same as in Figure 3.

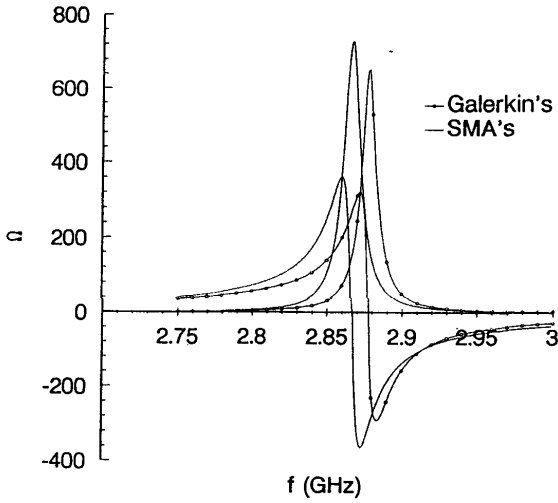


Figure 5. Input impedance comparison of an annular ring patch operating in  $TM_{11}$ . Parametric values are the same as in Figure 3 except  $b = 1.05a_1$ .  $M = 1, P = 0$ , and  $N = 1$  are used in Galerkin's method.

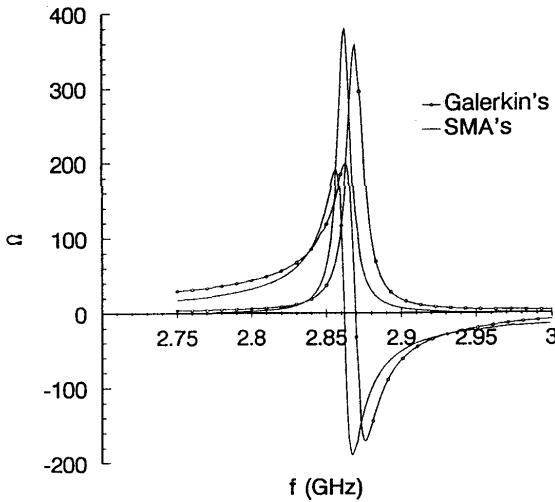
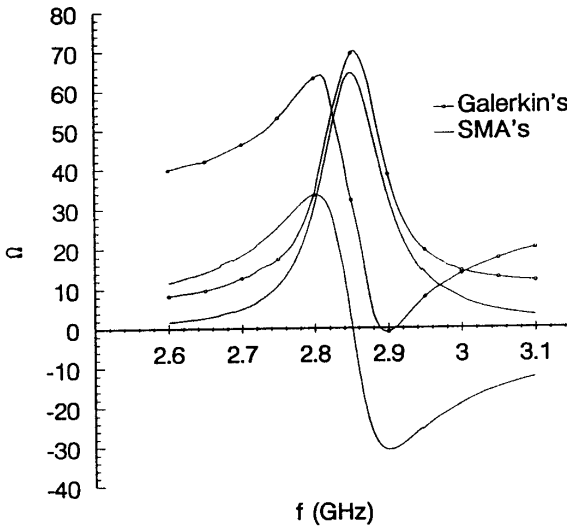


Figure 6. Input impedance comparison of an annular ring patch operating in  $TM_{21}$ .  $R = 0.1 \text{ mm}, a_1 = 14 \text{ mm}, a_2 = 2a_1, d = 0.05a_1, b = 1.05a_1, \epsilon_r = 2.65, \sigma = 5.8 \times 10^7, \tan \delta = 10^{-3}$ .  $M = 1, P = 0$ , and  $N = 2$  are used.

Figure 5 through Figure 7 show the comparison of the calculated input impedance between the Galerkin's method and the single mode approximation (SMA) method, which apply to the computation of different mode's operation. For comparison, Fig. 5 and Fig. 7 use the same parametric values as in Fig. 7 and Fig. 8 in reference [10], respectively. From Fig. 5 and Fig. 6, we note that the points where the reactance plots cross zero obtained by Galerkin's method are about 0.3% higher than that from the SMA method. This is because the SMA method depends on the assumption that the substrate thickness is nearly zero, while Galerkin's method does not have a harsh requirement on the substrate thickness. As indicated in [10], the resonant frequencies of  $TM_{n1}$  modes of the annular-ring structure increase monotonically versus the increasing of the substrate thickness. Therefore, when operating at such modes, the SMA method always yields a lower resonant frequency than that of the actual resonant frequency. From Fig. 8, where a much thicker substrate has been assumed in computation, we can see that the deviation between the two methods reaches 1.9% at such a  $d/a_1$  ratio.



**Figure 7. Input impedance comparison of an annular ring patch operating in  $TM_{12}$ .**  $R = 0.1$  mm,  $a_1 = 32$  mm,  $a_2 = 2a_1$ ,  $d = 0.05a_1$ ,  $b = 1.05a_1$ ,  $\epsilon_r = 2.65$ ,  $\sigma = 5.8 \times 10^7$ ,  $\tan \delta = 10^{-3}$ .  $M = 2$ ,  $P = 0$ , and  $N = 1$  are used.

As for Fig. 7, where the input impedance of the  $TM_{12}$  mode is plotted, we can see that the resistance plots agree well while the reactance plots shows some discrepancies. This is because that the SMA method does not include the inductance arising from the feed point while the Galerkin's method does [5,16].

In Figure 9, the convergence testing results have been presented, the various plots show the effects of increasing the number of basis functions in (25). We note that the deviation between the successive plots becomes less as the number of basis functions is increased, confirming the convergence of this method.

A number of experiments were carried out for the verification of the analysis. Figure 10.1 through Figure 12.1 show the comparison of the computed results using Galerkin's method with the measured ones, with the structure operated in  $TM_{11}$ ,  $TM_{21}$  and  $TM_{12}$  modes, respectively. The results obtained by using SMA method are also plotted for comparison, we note that the former is more close to the measured data than that of the later. The measurements were conducted in the HP8510B network analyzer. Figure 10.2 through Figure 12.2 are Smith-Chart plots produced in the network analyzer that indicates the measured input impedance of the microstrip annular ring antenna specified in Fig. 10.1 through Fig. 12.1, respectively. The measured data should be converted into the probe center since the readout data is the impedance at the interface of the connector. The distance, including an N-type to 3.5 mm adapter, between the calibrated interface and the probe center, by converting into the air-filled transmission line, is 37.7 mm. Convert the measured data point by point, the third curves in Fig. 10.1 through Fig. 12.1 can be obtained from Fig. 10.2 through Fig. 12.2, respectively.

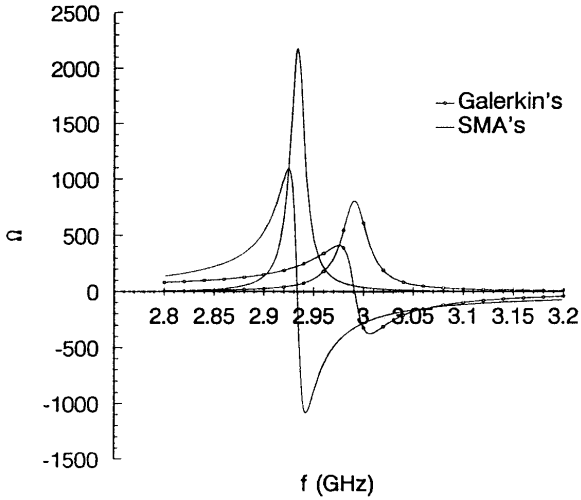


Figure 8. Input impedance comparison of an annular ring patch operating in  $TM_{11}$ . Parametric values are the same as used in Fig.5, except  $d = 0.2a_1$ . Again  $M = 1, P = 0$ , and  $N = 1$  are used.

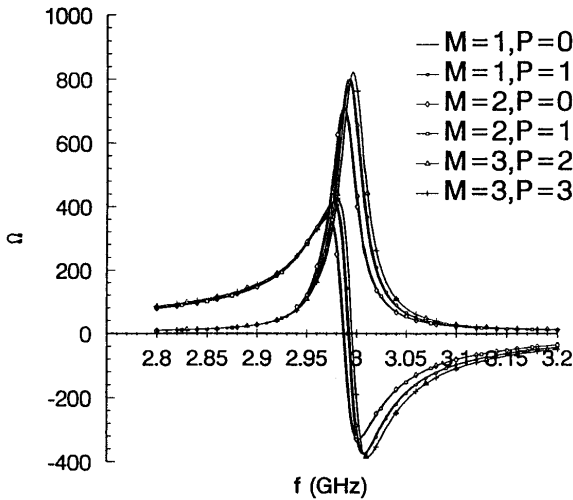


Figure 9. Plots showing the convergence of Galerkin's method for increasing number of basis function. Parametric values are the same as used in Figure 8.

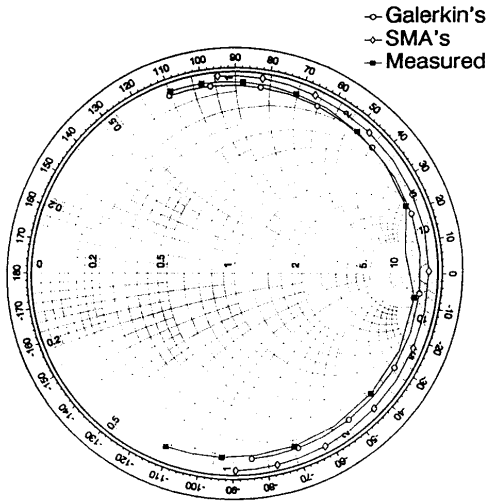


Figure 10.1. Input impedance comparison between computed and measured results for  $TM_{11}$  operation.  $R = 0.65$  mm,  $a_1 = 16.5$  mm,  $a_2 = 33.0$  mm,  $d = 2.0$  mm,  $b = 24.8$  mm,  $\epsilon_r = 2.95$ ,  $\sigma = 5.8 \times 10^7$ ,  $\tan \delta = 1.8 \times 10^{-3}$ .  $M = 1$ ,  $P = 0$ , and  $N = 1$  are used in Galerkin's method,  $f = 1.1 \sim 1.3$ . step=20 MHz.

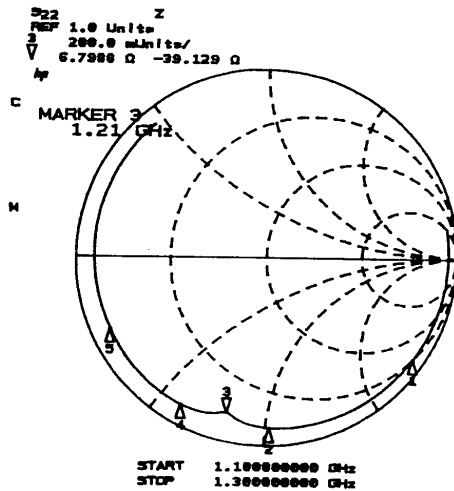


Figure 10.2. Smith-Chart plot of input impedance measured in HP8510B Network Analyzer,  $TM_{11}$  operation. The coaxial adapter should be taken into account for comparison with the computed results shown in Figure 10.1.

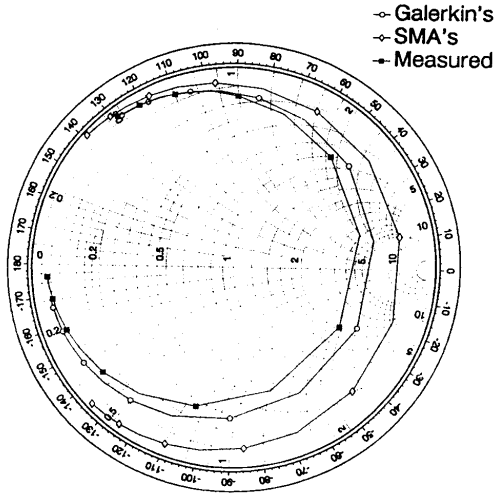


Figure 11.1. Input impedance comparison between computed and measured results for  $TM_{21}$  operation.  $R = 0.65$  mm,  $a_1 = 32.0$  mm,  $a_2 = 64.0$  mm,  $d = 2.0$  mm,  $b = 34.0$  mm,  $\epsilon_r = 2.95$ ,  $\sigma = 5.8 \times 10^7$ ,  $\tan \delta = 1.8 \times 10^{-3}$ .  $M = 1$ ,  $P = 0$ , and  $N = 2$  are used in Galerkin's method,  $f = 1.15 \sim 1.25$  GHz, step=10 MHz.

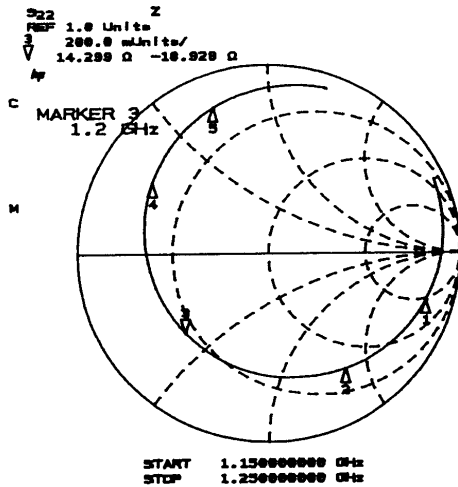


Figure 11.2. Smith-Chart plot of input impedance measured in HP8510B Network Analyzer,  $TM_{21}$  operation. The coaxial adapter should be taken into account for comparison with the computed results shown in Figure 11.1.

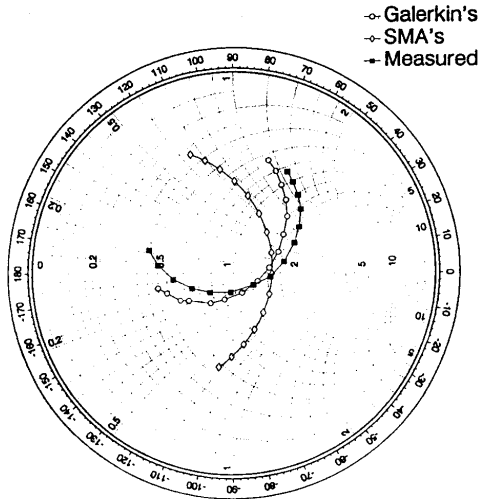


Figure 12.1. Input impedance comparison between computed and measured results for  $TM_{12}$  operation. Parametric values are the same as used in Fig.11.1.  $M = 2$ ,  $P = 0$ , and  $N = 1$  are used in Galerkin's method,  $f = 2.58 \sim 2.72$  GHz, step=10 MHz.

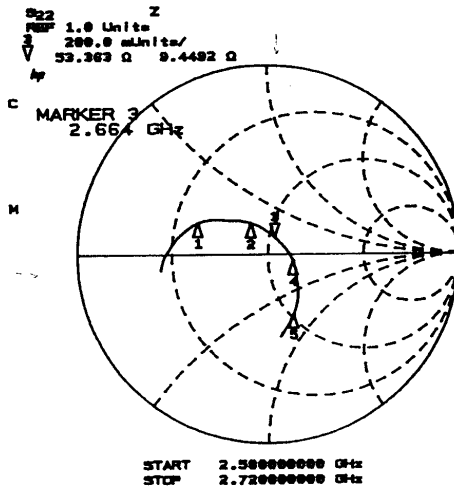


Figure 12.2. Smith-Chart plot of input impedance measured in HP8510B Network Analyzer,  $TM_{12}$  operation. The coaxial adapter should be take into account for comparison with the computed results shown in Figure 12.1.

## 8. Conclusion

In the above, we used the current on the surface of the probe as the primary source to determine the induced current on the microstrip annular ring patch. The dyadic Green's function in stratified media has been employed in order to account for the surface wave. The current on both the probe and the patch has been taken into account in obtaining the input impedance. Numerical experiments show that the above analytical procedure yields good convergent result even in the case of thick substrate. Measurement concerning the input impedance have been conducted to verify the analysis. The measured data show that this analytical procedure significantly improves the accuracy in the input impedance computation of the microstrip annular ring antennas in comparison with the single mode approximation method.

## Appendix A

Consider a probe of radius  $R$  with uniform  $z$ -directed current  $I$  radiating between two parallel plates. There is only outgoing radiation since reflection is absent. For  $e^{-i\omega t}$  dependent the field is given by [15]

$$\begin{aligned} E_{1z}^S &= \frac{\omega\mu I}{2\pi i} \int_0^\infty dk_\rho k_\rho \frac{J_0(k_\rho R)J_0(k_\rho \rho)}{k_{1s}^2 - k_\rho^2} \\ &= -\frac{\omega\mu I}{4} J_0(k_{1s}R)H_0^{(1)}(k_{1s}\rho), \quad \rho < R \end{aligned} \quad (\text{A1})$$

We have used superscript  $S$  to denote the singular nature of the field at  $\rho = 0$ . For a probe displace to  $\rho = xb$ , the use of the addition theorem[18] shows that the field is given by

$$\begin{aligned} E_{1z}^s &= -\frac{\omega\mu I}{4} J_0(k_{1s}R) \sum_{n=0}^{\infty} (2 - \delta_{0n}) \cos n\phi \\ &\cdot \begin{cases} H_n^{(1)}(k_{1s}b)J_n(k_{1s}\rho), & \rho < b \\ J_n(k_{1s}b)H_n^{(1)}(k_{1s}\rho), & \rho > b \end{cases} \end{aligned} \quad (\text{A2})$$

In the case of an annular-ring patch printed on the upper surface, instead of the infinite large metallic plate, magnetic walls are present

at  $\rho = a_1$  and  $\rho = a_2$  reflected waves are generated giving the field as

$$E_{1z}^s = -\frac{\omega\mu I}{4} J_0(k_{1s}R) \sum_{n=0}^{\infty} (2 - \delta_{0n}) \cos n\phi$$

$$\cdot \begin{cases} H_n^{(1)}(k_{1s}b)J_n(k_{1s}\rho) + A_n J_n(k_{1s}\rho) + B_n N_n(k_{1s}\rho), & \rho < b \\ J_n(k_{1s}b)H_n^{(1)}(k_{1s}\rho) + A_n J_n(k_{1s}\rho) + B_n N_n(k_{1s}\rho), & \rho > b \end{cases} \quad (\text{A3})$$

By requiring that the tangential **H**-field be zero at  $\rho = a_1$ ,  $\rho = a_2$ , namely,

$$\frac{\partial E_z}{\partial \rho} = 0, \quad \rho = a_1, a_2$$

we have

$$\left. \begin{aligned} H_n^{(1)}(k_{1s}b)J'_n(k_{1s}a_1) + A_n J'_n(k_{1s}a_1) + B_n N'_n(k_{1s}a_1) &= 0 \\ J_n(k_{1s}b)H_n^{(1)'}(k_{1s}a_2) + A_n J'_n(k_{1s}a_2) + B_n N'_n(k_{1s}a_2) &= 0 \end{aligned} \right\} \quad (\text{A4})$$

from (A4),  $A_n$  and  $B_n$  can be expressed as

$$\left. \begin{aligned} A_n &= \frac{J_n(k_{1s}b)H_n^{(1)'}(k_{1s}a_2)N'_n(k_{1s}a_1) - H_n^{(1)}(k_{1s}b)J'_n(k_{1s}a_1)N'_n(k_{1s}a_2)}{J'_n(k_{1s}a_1)N'_n(k_{1s}a_2) - J'_n(k_{1s}a_2)N'_n(k_{1s}a_1)} \\ B_n &= \frac{H_n^{(1)}(k_{1s}b)J'_n(k_{1s}a_2) - J_n(k_{1s}b)H_n^{(1)'}(k_{1s}a_2)}{J'_n(k_{1s}a_1)N'_n(k_{1s}a_2) - J'_n(k_{1s}a_2)N'_n(k_{1s}a_1)} J'_n(k_{1s}a_1) \end{aligned} \right\} \quad (\text{A5})$$

We can Still rewrite (A3) as

$$\begin{aligned}
E_{1z}^S &= \sum_{n=0}^{\infty} (2 - \delta_{0n}) \cos n\phi \frac{\omega\mu I}{2\pi i} \int_0^{\infty} dk_{\rho} k_{\rho} \frac{J_0(k_{\rho}R)J_n(k_{\rho}b)J_n(k_{\rho}\rho)}{k_{1s}^2 - k_{\rho}^2} \\
&\quad - \frac{\omega\mu I}{4} \sum_{n=0}^{\infty} (2 - \delta_{0n}) \cos n\phi J_0(k_{1s}R) [A_n J_n(k_{1s}\rho) + B_n N_n(k_{1s}\rho)]
\end{aligned} \tag{A6}$$

The transverse magnetic field in the cavity can be expressed as ([15], p.215)

$$\mathbf{H}_{1s} = \frac{-i\omega\varepsilon_1}{k_1^2 - k_{1z}^2} \nabla_s \times \hat{z} E_{1z}^S \tag{A7}$$

In the above,  $k_{1z}$  equals zero if we only consider the dominant mode in the cavity. The surface current on the patch can then be obtained as

$$\mathbf{J}_s^S = \mathbf{n} \times \mathbf{H}_{1s} = -\hat{z} \times \mathbf{H}_{1s} \tag{A8}$$

Substitute (A7) into (A8), we have

$$\mathbf{J}_s^S = \frac{i\omega\varepsilon_1}{k_1^2} \hat{z} \times \nabla_s \times \hat{z} E_{1z}^S = \frac{i\omega\varepsilon_1}{k_1^2} \nabla_s E_{1z}^S \tag{A9}$$

Substitute (A6) into (A9), we have

$$\begin{aligned}
\mathbf{J}_s^S &= \frac{I}{2\pi} \sum_{n=0}^{\infty} (2 - \delta_{0n}) \int_0^{\infty} dk_{\rho} k_{\rho}^2 \frac{J_0(k_{\rho}R)J_n(k_{\rho}b)}{k_{1s}^2 - k_{\rho}^2} \\
&\quad \cdot \left( \hat{\rho} \cos n\phi J'_n(k_{\rho}\rho) - \hat{\phi} \sin n\phi \frac{n}{k_{\rho}\rho} J_n(k_{\rho}\rho) \right) \\
&\quad - \frac{I}{4} i k_{1s} J_0(k_{1s}R) \\
&\quad \sum_{n=0}^{\infty} (2 - \delta_{0n}) \left( \hat{\rho} \cos n\phi f'_n(k_{1s}\rho) - \hat{\phi} \sin n\phi \frac{n}{k_{1s}\rho} f_n(k_{1s}\rho) \right)
\end{aligned} \tag{A10}$$

where

$$\begin{aligned}
f_n(k_{1s}\rho) &= A_n J_n(k_{1s}\rho) + B_n N_n(k_{1s}\rho) \\
f'_n(k_{1s}\rho) &= A_n J'_n(k_{1s}\rho) + B_n N'_n(k_{1s}\rho)
\end{aligned}$$

In general, we can write the conjugate current on the electric patch as

$$\begin{aligned} \mathbf{k}_n^S(\rho) = & \frac{I}{2\pi}(2 - \delta_{0n}) \int_0^\infty dk_\rho k_\rho^2 \frac{J_0(k_\rho R) J_n(k_\rho b)}{k_\rho^2 - k_{1s}^2} \cdot \left[ \begin{array}{c} J'_n(k_\rho \rho) \\ \frac{n}{k_\rho \rho} J_n(k_\rho \rho) \end{array} \right] \\ & + \frac{I}{4}(2 - \delta_{0n}) i k_{1s} J_0(k_{1s} R) \left[ \begin{array}{c} f'_n(k_{1s} \rho) \\ \frac{n}{k_{1s} \rho} f_n(k_{1s} \rho) \end{array} \right] \end{aligned} \quad (\text{A11})$$

Apply the vector Hankel transform on Eq. (A11), we have

$$\begin{aligned} \mathbf{K}_n^S(k_\rho) = & \frac{I}{2\pi}(2 - \delta_{0n}) \frac{k_\rho J_0(k_\rho R) J_n(k_\rho b)}{k_\rho^2 - k_{1s}^2} \left[ \begin{array}{c} 1 \\ 0 \end{array} \right] \\ & + \frac{I}{4}(2 - \delta_{0n}) i k_{1s} J_0(k_{1s} R) \left[ \begin{array}{c} K_n^{(1)}(k_\rho) \\ K_n^{(2)}(k_\rho) \end{array} \right] \end{aligned} \quad (\text{A12a})$$

where

$$K_n^{(1)}(k_\rho) = \frac{k_\rho G_n(k_\rho) - k_{1s} F'_n(k_\rho)}{k_\rho^2 - k_{1s}^2} \quad (\text{A12b})$$

$$K_n^{(2)}(k_\rho) = \frac{n}{k_{1s} k_\rho} F_n(k_\rho) \quad (\text{A12c})$$

$$G_n(k_\rho) = a_2 f'_n(k_{1s} a_2) J_n(k_\rho a_2) - a_1 f'_n(k_{1s} a_1) J_n(k_\rho a_1)$$

$$F_n(k_\rho) = f_n(k_{1s} a_2) J_n(k_\rho a_2) - f_n(k_{1s} a_1) J_n(k_\rho a_1)$$

$$F'_n(k_\rho) = a_2 f_n(k_{1s} a_2) J'_n(k_\rho a_2) - a_1 f_n(k_{1s} a_1) J'_n(k_\rho a_1)$$

When we choose  $k_{1s}$  that is close to the wave number of the magnetic wall cavity filled with lossy dielectric medium, and recall from Eq. (14), we can conclude that

$$J'_n(k_{1s} a_1) N'_n(k_\rho a_2) - J'_n(k_{1s} a_2) N'_n(k_\rho a_1) \cong 0 \quad (\text{A13})$$

thereby

$$f'_n(k_{1s} a_2) \cong 0, \quad \text{and} \quad f'_n(k_{1s} a_1) \cong 0 \quad (\text{A14})$$

Therefore Eq. (A5) can still be simplified as

$$\left. \begin{aligned} A_n &= iN'_n(k_{1s}a_2) \frac{J_n(k_{1s}b)N'_n(k_{1s}a_1) - N_n(k_{1s}b)J'_n(k_{1s}a_1)}{J'_n(k_{1s}a_1)N'_n(k_{1s}a_2) - J'_n(k_{1s}a_2)N'_n(k_{1s}a_1)} \\ B_n &= -iJ'_n(k_{1s}a_1) \frac{J_n(k_{1s}b)N'_n(k_{1s}a_2) - N_n(k_{1s}b)J'_n(k_{1s}a_2)}{J'_n(k_{1s}a_1)N'_n(k_{1s}a_2) - J'_n(k_{1s}a_2)N'_n(k_{1s}a_1)} \end{aligned} \right\} \quad (\text{A15})$$

The first term in Eq. (A12b) tends to be zero, thus (A12b) can also be simplified as

$$K_n^{(1)}(k_\rho) = \frac{-k_{1s}F'_n(k_\rho)}{k_\rho^2 - k_{1s}^2} \quad (\text{A16})$$

Hitherto, the field in the annular-ring cavity together with the induced current on the patch produced by the probe current have been obtained.

## Acknowledgment

The author sincerely thanks Dr. Robert Paknys in Concordia University of Montreal for his generous offering of the program relating to the computation of Hankel's functions with complex arguments.

## References

1. Carver, K. R., and J. W. Mink, "Microstrip antenna technology," *IEEE Trans.*, Vol. AP-29, 2–24, 1981.
2. Lo, Y. T., D. Solomon, and W. F. Richards, "Theory and experiment on microstrip antennas," *IEEE Trans.*, Vol. AP-27, 137–145, 1979.
3. Rana, I. E., and N. G. Alexopoulos, "Current distribution and input impedance of printed dipoles," *IEEE Trans.*, Vol. AP-29, No. 1, 99–105, 1981.
4. Chew, W. C., and J. A. Kong, "Resonance of non-axial symmetric modes in microstrip disk resonators," *J. Math. Phys.*, Vol. 21, 2590–2598, 1980.
5. Chew, W. C., and J. A. Kong, "analysis of a circular microstrip disk antenna with a thick dielectric substrate," *IEEE Trans.*, Vol. AP-29, No. 1, 68–76, Jan. 1981.

6. Tulintseff, A. N., S. M. Ali, and J. A. Kong, "Input impedance of a probe-fed stacked circular microstrip antenna," *IEEE Trans.* Vol. AP-39, No. 3, 381–390, 1991.
7. Bhattacharyya, A. K., and R. Garg, "Input impedance of annular ring microstrip antenna using circuit theory approach," *IEEE Trans.*, Vol. AP-33, 369–374, 1985.
8. Bhattacharyya, A. K., and R. Garg, "Spectral domain analysis of wall admittance for circular and annular microstrip patches and the effect of surface waves," *IEEE Trans.*, Vol. AP-33, 1067–1073, 1985.
9. Nurie, N. S., and R. J. Langley, "Input impedance of concentric ring microstrip antennas for dual frequency band operation including surface wave coupling," *IEE Proc. H*, Vol. 137, No. 6, 331–336, Dec. 1990.
10. Ali, S. M., W. C. Chew, and J. A. Kong, "Vector Hankel transform analysis of annular ring microstrip antenna," *IEEE Trans.*, Vol. AP-30, No. 4, 637–644, July 1982.
11. Nie, Z., W. C. Chew, and Y. T. Lo, "analysis of the annular-ring loaded circular-disk microstrip antenna," *IEEE Trans.*, AP-38, No. 6, 806–813, 1990.
12. Wu, Y. S., and F. J. Rosenbaum, "Mode chart for microstrip ring resonators," *IEEE Trans.*, Vol. MTT-21, 457–489, 1973.
13. Mink, J. W., "Circular ring microstrip antenna," *IEEE Trans.*, Vol. AP-30, 605–608, 1982.
14. Chew, W. C., *Waves and Fields in Inhomogeneous Media*, Van Nostrand Reinhold, New York, 1990.
15. Kong, J. A., *Theory of Electromagnetic Waves*, New York, Wiley-Interscience, 1975.
16. Zheng, J. X., and D. C. Chang, "End-correction network of a coaxial probe for microstrip patch antennas," *IEEE Trans.*, Vol. AP-39, No. 1, Jan., 115–118, 1991.
17. James, J. R., and P. S. Hall, Ed., *Handbook of Microstrip Antenna*, Peter Peregrinus Ltd., London, 1989
18. Abramowity, M., and I. Stegun, *Handbook of Mathematical Functions*, New York, Macmillan, 1968
19. Zhong, S.-S., *Microstrip Antennas, Theory and Application*, Published by Xi'an Electronic Technology University, Xi'an, China, 1991.

20. Paknys, R., "Evaluation of Hankel functions with complex argument and complex order," *IEEE Trans.* Vol. AP-40, No. 5, 569–578, 1992.
21. Mosig, J. R., and F. E. Gardiol, "General integral equation formulation for microstrip antennas and scatterers," *Proc.IEE*, Pt. H, Vol. 132, 424–432, 1985.
22. Watson, G. N., *A Treatise on the Theory of Bessel Functions*, 2nd ed., New York, Pergamon Press, 1944.
23. Sneddon, I. N., *Mixed Boundary Value Problems in Potential Theory*, Wiley, New York, 1966.